Z. Phys. A – Atoms and Nuclei 322, 149–156 (1985)

Zeitschrift für Physik A Atoms and Nuclei

Density Distributions in Nuclei

V.M. Strutinsky, A.G. Magner, and V.Yu. Denisov
Institute for Nuclear Research, Kiev, USSR

Received January 14, 1985

Density distribution across the nuclear surface is obtained in the approximation of relatively sharp nuclear edge. It is used to determine dynamical parts of the density relevant to density vibration resonances. Results of the simple calculations are in close agreement with detailed microscopic theories.

PACS: 21.10.Gv; 21.10.Re; 21.60.Ev

1. Introduction

Simple and accurate solution of some problems involving nuclear density distributions uses the notion of an effective sharp surface [1, 2]. It exploits the property of saturation, which is a characteristic feature of nuclei. The realistic energy density distribution is minimal at a certain density of nucleons corresponding to infinite matter [3]. As a result, relatively narrow edge region exists in finite nuclei in which the density drops sharply from its central value to zero. The effective surface is introduced according to locations of points of maximal density gradient. Position of the surface may vary in time in accordance with dynamics of the density distribution. The coordinate system related to the surface is defined in such a way that one of the spacial coordinates (ξ) is the distance from the given point to the surface. This coordinate system is conveniently used in the region of nuclear edge allowing for an easy extraction of relatively large terms in the density distribution equations. Neglecting the other contributions, sum of such terms leads to a simple one-dimensional equation (in spacial coordinates, at least) which determines approximately the density distribution in the region of diffused nuclear surface. When this edge distribution of the density is known static and dynamical density distributions which correspond to diffused surface conditions can be easily constructed. To do so, one has, however, to determine the dynamics of the effective surface which is coupled to volume dynamics of the density by certain boundary conditions [2, 4]. It is of interest to check the accuracy of effective surface approximation by compairing the results with the existing detailed – and uncomparably more involved – theories.

2. Statics

The total energy is represented in the form

$$\mathscr{E}(\rho)=-b_v\rho+\rho\varepsilon(\rho)+\left(\beta+\frac{\gamma}{4\rho}\right)(\nabla\rho)^2+\kappa\Delta\rho, \tag{1}$$

where b_v is the energy of separation of a particle in the infinite matter, b_v, β, γ and κ are positive constants. Being a function of local density ρ, $\varepsilon(\rho)$ corresponds to saturation condition,

$$d\varepsilon(\bar{\rho})/d\rho=0. \tag{2}$$

The quantity $\bar{\rho}$ is the equilibrium density for nuclear matter and, according to its definition in (1),

$$\varepsilon(\bar{\rho})=0. \tag{3}$$

In addition, the particle binding energy in uniform matter should equal zero at $\rho\to 0$,

$$-b_v+\varepsilon(0)=0. \tag{4}$$

The equilibrium density distribution is determined

by variational Lagrange equation

$$\frac{d}{d\rho}(\rho\varepsilon(\rho))-2\left(\beta+\frac{\gamma}{4\rho}\right)\Delta\rho+\frac{\gamma}{4\rho^2}(\nabla\rho)^2+\lambda=0, \qquad (5)$$

in which λ is the Lagrange factor for the condition that the total number of particles A is fixed. It represents a finite size correction to separation energy. Note, that the presence of $\Delta\rho$-term in (1) does not affect the equilibrium density distribution. In the nuclear volume terms of (5) containing derivatives of ρ are small. They are large near the nuclear edge where the ξ-coordinate can be conveniently used. The largest terms in the equation are in this region proportional to $1/a^2$ where a is the thickness of the diffused edge and by requiring that their sum should vanish the following equation is obtained after some transformations [2],

$$d\rho/d\xi=-2\rho\varepsilon^{1/2}(\rho)(4\beta\rho+\gamma)^{-1/2}. \qquad (6)$$

($\xi=+\infty$ at large distances and $\xi=0$ at the surface.) It determines the density distribution in the edge region across the effective surface. The shape of the surface is arbitrary so far. It is only required that a should be small in comparison with the local value of the mean curvature radius of the surface. To determine the surface part of the total energy one writes the total energy corresponding to (1) as

$$E=-b_v A+\int d^3r[\rho\varepsilon(\rho)+(\beta+\gamma/4\rho)(\nabla\rho)^2] \qquad (7)$$

and, taking (6) into account, it is noted that both items in square brackets contain $(d\rho/d\xi)^2$ which becomes large in the edge region. Keeping only such terms provides a sufficient accuracy: More accurate approximations would lead to $A^{1/3}$-terms in energy which are of no significance here. The two items in the integral in (7) produce then equal contributions and the integral itself can approximately be expressed as a surface integral taken across the surface of maximal density gradient. It is obtained, then,

$$E=E_v+E_s+\mathcal{O}(A^{1/3})$$

where

$$E_v=-b_v A \qquad (8)$$

is the volume energy and the surface energy is

$$E_s=\sigma S, \qquad (9)$$

where S is the area of the effective surface. The surface tension constant

$$\sigma=2\int_{-\infty}^{+\infty} d\xi(\beta+\gamma/4\rho)(d\rho/d\xi)^2, \qquad (10)$$

where the derivative is taken along perpendicular to the surface and the integration is also performed in this direction, see also in [2, 5]. It can be noted that unambigous definition of the surface energy can be given only within this semi-classical model. It cannot be obtained, for example, in Hartree-Fock derivations when the energy (7) contains single-particle shell effects. In such cases averagings can be applied such as used in shell correction calculations [6]. Otherwise the surface energy term can be seriously misestimated.

Terms in (1) and (7) containing parameters γ and κ appear there as quantal corrections to the Thomas-Fermi kinetic energy, and are both proportional to $\hbar^2$. So,

$$\gamma=\frac{\hbar^2}{18m} \qquad (11)$$

where m is the nucleon mass. The amplitude of this term is known to be too small to reproduce the empirical surface energy. The presence of the other surface term which is not singular at $\rho\to 0$ is presently argued on the ground of some Skyrme-force arguments. It is believed, however, that such a term presents a general macroscopic feature of any dense system of particles. In this way a non-local component of energy density is represented due to interaction of adjacent volume elements of different densities. If so, it needs not to be necessaryly related to the Skyrme-force approach. The volume part, $\varepsilon(\rho)$, can also be determined from general arguments with a sufficient accuracy, particularly in view of the fact that – as these calculations also show – many essential results are not sensitive to the specific form of $\varepsilon(\rho)$.

For further derivations it is convenient to use demensionless quantities by writting

$$\rho=\bar{\rho}y \qquad (12)$$

and

$$\varepsilon(\rho)=b_v\varepsilon(y), \qquad (13)$$

where $\varepsilon(y)$ is dimensionless, in contrast to $\varepsilon(\rho)$. The unit of distance is

$$a=(4\beta\rho/b_v)^{1/2}=(3\beta/\pi r_0^3 b_v)^{1/2}, \qquad (14)$$

where r_0 is defined by relationship

$$\bar{\rho}=3/4\pi r_0^3. \qquad (15)$$

Equation (6) takes then the form

$$dy(x)/dx=-2y\varepsilon^{1/2}(y)/(c+y)^{1/2}, \qquad x=\xi/a, \qquad (16)$$

and it contains dimensionless parameter

$$c=\gamma/4\beta\bar{\rho}=2.41 r_0^3/\beta, \tag{17}$$

see (11, 15). The energy here is expressed in MeV and distance is in Fermis. Values of c fitting the surface energy are small ($c<0.1$) and it makes it possible to obtain particularly simple analytical solution which is described below. With the phenomenological values [7] of $b_v=16$ MeV and $r_0=1.2$ fm ($\bar{\rho}=0.15$ fm^{-3}) one has

$$c=4.0\beta^{-1}, \tag{18}$$

and

$$a=0.19\beta^{1/2}\ \text{fm}. \tag{19}$$

The surface energy is determined by parameter

$$b_s=4\pi r_0^2\sigma=(27 b_v\beta/4\pi r_0^5)^{1/2} J, \tag{20}$$

where

$$J=\int_{-\infty}^{+\infty} dx(dy(x)/dx)^2(1+c/y)$$
$$=2\int_0^1 dy(c+y)^{1/2}\varepsilon^{1/2}(y). \tag{21}$$

Solution $y(x)$ to (6) which is of interest to us turns into zero asymptotically (or exactly, if $c=0$) at some positive value of x off the nuclear surface. The surface itself is positioned at $x=0$ and is determined by the condition that the density gradient is maximal there, that is,

$$d^2 y(0)/dx^2=0. \tag{22}$$

From this condition and (16) some algebraic equation is obtained which determines a certain value of $y=y_0$ corresponding to maximal gradient,

$$\varepsilon(y_0)(2c+y_0)+(c+y_0)\, y_0\, d\varepsilon(y_0)/dy=0.$$

The equation is resolved numerically for any given $\varepsilon(\rho)$ and it provides then the boundary condition,

$$y(0)=y_0, \tag{23}$$

which determines uniquely the sought physical solution to (5, 16).

For small values of c such as are of interest to applications the solutions depend weekly on this parameter. Another significant feature of solutions is their remarkable insensitivity to details of $\varepsilon(\rho)$. As a result, solutions to (16) turn out to be close to a certain universal shape function, see Fig. 1. The fat lines there show the shape function $y(x)$ determined

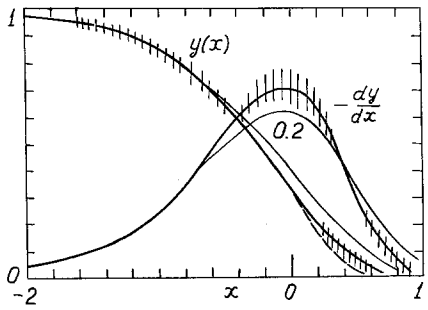

Fig. 1. Shaded regions represent solutions to (16) for various versions of effective energy density function $\varepsilon(y)$ derived with values of β currently attached to each version ($c<0.1$). Thin lines correspond to $c=0.2$. Fat lines correspond to parabolic $\varepsilon(y)$, see (24) and broken lines correspond to asymptotic solution (25). They can be accepted as universal practical solutions

for parabolic

$$\varepsilon(y)=(1-y)^2. \tag{24}$$

Closed form solution for $y(x)$ corresponding to this case can be found if either β or c equals zero. For $c=0$ (version Par) one has

$$y(x)=\text{th}^2(x-0.658), \tag{25}$$

where the boundary condition (22, 23) is satisfied. This solution turns into 1/3 at the maximal gradient point at $x=0$ and is identically zero for $x\geqq 0.658$. Parabolic

$$\varepsilon(\rho)=(K/18\bar{\rho}^2)(\rho-\bar{\rho})^2 \tag{26}$$

determines, by means of (4), the compressibility modulus K as related to phenomenological binding energy parameter b_v, namely,

$$K=18 b_v, \tag{27}$$

and its value $K=290$ MeV found in this way agrees with what is obtained from fitting the monopole resonance energies in the first-sound model.

Equation (25) can be compared with the Thomas-Fermi quantity ($\beta=0$ and $c=\infty$) which, for parabolic $\varepsilon(\rho)$, is

$$\rho(r)=\bar{\rho}(1+\exp((r-R)/\alpha))^{-1}, \tag{28}$$

where

$$\alpha=\tfrac{1}{2}(18\gamma/K)^{1/2},$$

see also [7, 8]. The gradient of ρ is maximal at $r=R$, where $\rho=\frac{1}{2}\bar{\rho}$, and $d\rho/dr$ is symmetric relative

to this point. The surface energy parameter is now

$$b_s = \tfrac{3}{2}(b_v \gamma)^{1/2}/r_0 \tag{29}$$

and it equals 7.6 MeV (i.e., too little) for the standard value of $b_v = 16$ MeV.

Very specific feature of solutions to (16) at smaller c-values is the asymmetry of $y'(x)$ relative to the maximum point at $x=0$: The density approaches its central value significantly more slowly than zero off the surface. It might seem to be the result of relative softness of nuclear matter in the volume but it is not the case. This asymmetry of $y'(x)$ is the consequence of the form of surface term in (1) at $\beta \neq 0$. It can be seen, particularly, in comparison with the Thomas-Fermi case ($\beta=0$), when $y'(x)$ is either exactly (for (28)) or nearly symmetric function. Closed form solutions to (6) corresponding to parabolic $\varepsilon(\rho)$, $c=0$ or ∞ and not considering initial conditions which determine position of the effective surface, were discussed for the case of semi-infinite matter in [1, 8–10]. The apparent asymmetry of such a solution in [10] which seemingly contradicts our conclusion was entirely due to the absence there of formal definition of the surface and the related ambiguity in definition of the point $x=0$. The noted weak dependence of $y(x)$ on specific forms of $\varepsilon(\rho)$ cannot be explained as trivial consequence of the fact that all Skyrme forces are so fitted that they reproduce approximately the same functional dependence on ρ. That it was not so was seen in many calculations. Instructive is the following example of the energy density

$$\varepsilon(\rho) = f\rho^p - g\rho^q + b_v, \quad (p>q; f, g>0). \tag{30}$$

The corresponding

$$\varepsilon(y) = 1 + (q y^p - p y^q)/(p-q)$$

and

$$d\varepsilon(y)/dy = pq(y^p - y^q)/((p-q)y),$$

do not depend on coefficients f and g in (30). So, the distribution function $y(x)$ is also independent on these quantities, according to (16). The coefficients in (26, 30) appear only in scale transformation factor (14) and in (17). Also the effect of even significant variations of p and q is rather small. Noticeable asymmetry of dy/dx arises only for unrealistically small values of $q<0.5$ in the negative (attraction) term in (30).

Some quantitative characteristics related to shape of $y(x)$ are shown in Table 1. Shape of the density distribution in the edge region is characterized in a compact form by integral

$$\bar{x} = \int_{-\infty}^{+\infty} x\,dx(dy/dx) \tag{31}$$

and

$$\Delta x = (\overline{x^2} - \bar{x}^2)^{1/2}, \tag{32}$$

where

$$\overline{x^2} = \int_{-\infty}^{+\infty} x^2\,dx(dy/dx).$$

Quantity $\bar{x}$ represents the above mentioned asymmetry and Δx determines the width of the transition region. Derived with various effective forces, these quantities are shown in first two lines in Table 1. They are to be multiplied by scale factor (19) in order to obtain them in the usual dimension. The third line presents surface energy integrals (21) and in the next line are shown the surface energy constants (20) obtained with the values of β presently attached to each effective force. The values of b_s are widely spread, which is believed to be due to absence of proper definition of the surface energy in the original papers where β-parameter was defined. So, the next line presents values of β which, for each version of $\varepsilon(\rho)$, would provide correct surface energy parameter $b_s = 19$ MeV.

The results of this section allow for another independent determination of β based on consideration of the density distribution. Indeed, as it can be seen in Fig. 1, the maximal slope of $y(x)$ equals 0.65–0.75 and varies little depending on the form of $\varepsilon(\rho)$. The

Table 1. Integrals (31, 32, 21) for different versions of Skyrme forces, EHP is for $\varepsilon(\rho)$ of [14] and Par is for parabolic $\varepsilon(y)$, see (24). Other lines are explained in the text

	S I; S III; EHP	S II; S IV	S V	Sk_a	Sk-M; Par
$\bar{x}$	0.24–0.26	0.26–0.28	0.28–0.29	0.31–0.33	0.36–0.37
Δx	0.54–0.52	0.56–0.54	0.57–0.56	0.61–0.59	0.65–0.63
J	0.65–0.61	0.63–0.60	0.61–0.59	0.59–0.56	0.55–0.53
b_s	16.5; 18; 27	22; 26	28	22	18; –
β_{cor}	65	69	72	78	89

slope of the density in the edge region is then, by means of (19),

$$\frac{d\rho(R)}{dr}=\frac{\bar{\rho}}{a}\frac{dy(0)}{dx}\approx 0.13\text{–}0.15\,\beta^{-1/2},$$

and it can be compared with the measured slope of the charge distribution equal to $0.45\text{–}0.5\,\bar{\rho}\cdot\mathrm{fm}^{-1}$ [11]. It gives $\beta=60\text{–}70$ MeV · fm^5. This value of β would give correct surface energies with $\varepsilon(\rho)$ of S I-V forces [12, 13] and also with the energy functional of [14]. It differs, however, from many of the currently recommended values. For example, the original $\beta=40$ MeV · fm^5 in S I and 120 MeV · fm^5 in the version [14] of the energy functional.

Density distributions, calculated by means of (16), are compared in Fig. 2 with the ones obtained in detailed straightforward derivations performed in the frameworks of hydrodynamical and Hartree-Fock models. In each instance the energy functional was the same as in the reference quoted. The only free parameter in this figure was nuclear radius R in the scailing equation

$$r=R+ax. \tag{33}$$

It was determined by fitting the maximal density gradient point $y_0=0.35\text{–}0.38$ at $x=0$. It should be noted that with our definition of R it systematically accepts somewhat larger values (by 0.2–0.4 fm) than with the usual definition as one-half density point. Parameters β enter through (33, 19) and they were in each case the same as in the original versions of effective forces. Because the specific forms of $\varepsilon(\rho)$ are not important all edge-density distributions obtained in our derivations are essentially scale transforms (33), (19) of a certain universal shape function $y(x)$ such a shown in Fig. 1. Shallower density distribution in calculations with $\varepsilon(\rho)$ of [14] is due to unrealistically large value of $\beta=120$ MeV · fm^5 in this case.

The agreement is particularly close in comparisons with semi-classical derivations [14, 15]. Somewhat larger differences are observed in comparisons with quantal Hartree-Fock calculations. This can be expected because the Hartree-Fock densities contain single-particle shell effects in the nuclear volume and a quantal tail. Quantal long-range quasi-particle shell effects, which are due to multiple reflections in the potential well [16], disappear in semi-classical approximations such as considered here. Semi-classical models correspond to statistical averaging over a large range of single particle energies [17] and it is believed that shell effects can be obtained and included in the same way as in the shell correction derivations, see also in [6].

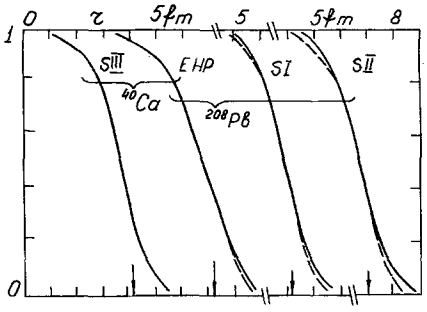

Fig. 2. Solid lines are the detailed calculations of edge density distributions for ^{40}Ca (two curves in the left side) and ^{208}Pb obtained with versions of $\varepsilon(\rho)$ indicated in the figure. Solid lines S I and S II are from [12] and they correspond to Hartree-Fock derivations. Other curves are results of classical model calculations with energy densities S III [15] EHP [14]. From left to right, $R=4.2$, 7.2 (4.2 for ^{40}Ca), 7.1, 6.8 Fermi. The second set of curves is the same for calcium and lead except for a radial shift. The results coincide, except where they are shown with broken lines

Knowing the distribution of density across the nuclear surface, reasonably accurate distribution of the density can be constracted for entire space for any given shape of the nuclear surface and, considering a moving surface, dynamics of the density distribution in the region of diffused surface can be described. Density dynamics inside the nuclear volume, where the density gradient is small, can be obtained as a separate problem and by fitting the two quantities together simple description of density dynamics can be obtained. Of special interest is the case of small amplitude vibrations.

3. Density Vibrations

For small amplitude vibrations, the time-dependent, or dynamical part of the density distribution can be approximately represented as sum of volume and surface components in the form

$$\rho_d(\mathbf{r}t)=\rho_v(\mathbf{r}t)\,y-\bar{\rho}\delta R(\theta t)\frac{dy(x)}{adx}. \tag{34}$$

Here, $y(x)$ is the shape function of Sect. 2 with the scale transformation (33), see also in [2]. The two items in (34) represent, correspondingly, the volume and surface dynamics. Note, that the surface term does not appear in the current density $\mathbf{i}(rt)$ which is described by usual equations of volume dynamics. However, rot $\mathbf{i}$ is proportional to dy/dx and is therefore, essentially a surface effect. For small distortions of spherical surface

$$\delta R(\theta t)=R\alpha_l(t)\,Y_{l0}(\theta). \tag{35}$$

Volume distortions of the density are described by wave equations of the 1st-sound or Landau-Silin kinetic equation (0th-sound), and for given multipolarity l

$$\rho_v(\mathbf{r}t)=\bar{\rho}a_l(t)\,j_l(kr)\,Y_{l0}(\theta). \tag{36}$$

Here, $a_l(t)$ is the amplitude of volume vibrations and j_l is spherical Bessel function [2, 4]. Relationships of this kind are valid for vibrations of the compression type (first-sound) as well as for semi-classical density vibrations in a quantal gas of interacting quasi-particles (zero-sound). The difference is only in values of wave number k which are to be found from certain boundary conditions for the volume problem and characteristic of each instance. The boundary conditions couple volume dynamics to movement of the surface and the result is that amplitude $a_l(t)$ and $\alpha_l(t)$ are proportional to each other,

$$\alpha_l(t)=\frac{1}{kR}\,j_l'(kR)\,a_l(t), \tag{37}$$

where primes mark derivatives taken with respect to the argument. By means of (37) the radial dependence in (34) can be factorized as

$$\rho_d(r)=j_l(kr)\,y(x)-(j_l'(kR)/ka)(dy(x)/dx) \tag{38}$$

where r and x are related through (33) and a is the scale factor (19). The boundary conditions are obtained from original equations assuming, particularly, the feature of large-gradient density at the surface [1, 2, 4, 5].

The volume dynamics is determined from one or another nuclear models. Among such the following two are believed to be of prime interest. So, it can be assumed that the local equilibration property pertains to collective density vibrations. (The first-sound model). Another possibility is the model of correlated oscillations of Fermi quasi-particles, which finds its theoretical foundation in Landau's theory of dense Fermi-liquid matter. In the semi-classical approximation the relevant equation for volume dynamics is the Landau's zero-sound equation for quasi-particle distribution function, see, e.g. [4]. Below in this section results are presented corresponding to these two different approaches.

3.A. *First-Sound Volume Vibrations*

The dynamical density for hydrodynamical droplet vibrations treated in approximation of effective dynamical surface was described in [2]. Here we present the results using more appropriate edge distribution functions of Sect. 2. The wave number k in (34, 38) is determined by characteristic equation for first-sound volume vibrations coupled to dynamical surface,

$$\frac{1}{kR}\,j_l'(kR)=(A^{1/3}K/3(l-1)(l+2)\,b_s)\,j_l(kR), \tag{39}$$

where K is the incompressibility modulus and b_s is the surface energy constant (20), see [2] and also [18].

In the left portion of Fig. 3 the distributions $\rho_d(r)$ derived according to (38, 39) (shown by broken lines) are compared with the corresponding detailed hydrodynamical calculations for ^{208}Pb [14, 19] and for $A=1{,}000$ [14]. The curves for $l=2$ are for convenience normalized to unity in the maxima. In our calculations the same $\mathscr{E}(\rho)$ and parameters β were used as in the referred detailed theories. Values of kR determined as roots of (39) are practically independent on specific value of the coefficient in r.h.s. of (39) as long as it remains large, which is the case. Combined with weak dependence of $y(x)$ on specific choice of $\varepsilon(\rho)$, a conclusion can be drawn that $\rho_d(r)$ is determined mainly by parameters R and β on which it depends in a simple scale-transform manner. Data presented in this portion of Fig. 3 cor-

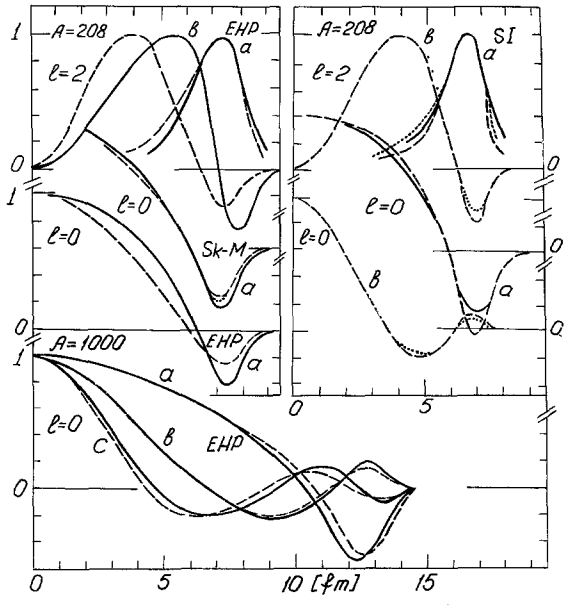

Fig. 3. Dynamic densities obtained in the present paper are indicated by broken and dotted lines wherever they differ from results of detailed calculations shown with solid lines. On the left, results of Sect. 3A are compared with hydrodynamical derivations using $\varepsilon(\rho)$ and β of EHP-model [14] and Sk-M [19]. Right figure presents comparisons of results of Sect. 3B with the RPA model of [20]. In the Fig. *a*, *b* and *c* correspond to first, second and third roots (resonances) of characteristic equations (39) and (40). Dotted lines correspond to exact solutions to (16), broken lines are obtained with asymptotic $y(x)$, Eq. (25)

respond to $R=7.3$ fm which was found from the condition that the total number of particles should equal 208 and it differs insignificantly from the same quantity determined for the static density distributions in [14, 19]. For $A=1{,}000$, $R=12.8$ fm. Curves a, b and c correspond to the first, second and third roots of (39) which equal, approximately: 3.12, 6.27, 9.42 for $l=0$, 0.512, 5.79 for $l=2$. Very close results were obtained with asymptotic solution (24) corresponding to parabolic $\varepsilon(\rho)$ according to (25).

The agreement between distributions $\rho_d(r)$ calculated in approximation of effective dynamic surface and boundary conditions and the ones obtained in detailed theories is rather close. Some difference is, however, noticed in comparison with the lead data of [14] for $l=2(b)$ and $l=0$ in the volume region which, apparently, is due to somewhat different radial dependences of the volume components. The wave number k determined in our calculations from characteristic equation (39) is, indeed, by 25–30% larger than effective value of k found in [14] for this case. On the other hand, no such discrepancy was seen in comparisons with Sk-M calculations for lead [19] and also in the data for $A=1{,}000$. On this ground it can be concluded that with the apparently too large $\beta=120$ MeV·fm^5 used in [14] the width of the diffused surface of the density is so large that it may inhance some inaccuracy of our approximation. Much closer agreement was, indeed, obtained with *HEP*-calculations using smaller, and more realistic values of β.

3.B. *Zero-Sound Volume Vibrations*

Collective density vibrations can also arise in a gas of correlated quasi-particles. In the approximation of zero-sound-plus-surface, the characteristic equation which determines eigen-values for the wave number k reads

$$\frac{1}{kR}\, j_l'(kR) = (3A^{1/3}\, e_F/(l-1)(l+2)\, b_s)((1-3s^2+G(s))\, j_l''(kR) + (1-s^2+\tfrac{1}{3}(2F_0+G(s)))\, j_l(kR)), \quad (40)$$

where e_F is the Fermi-energy. Parameter $s=v^{(0)}/v_F>1$ is the ratio of zero-sound velocity to velocity of quasi-particles and it is found from algebraic equation,

$$G(s)=F_0+s^2F_1(1+\tfrac{1}{3}F_1)^{-1}=\left(\frac{s}{2}\ln\frac{s+1}{s-1}-1\right)^{-1}. \quad (41)$$

Here, F_0 and F_1 are Landau's amplitudes of quasi-particle interaction in nuclear volume. Values of k obtained through (40, 41) lead to frequencies of eigen-modes which are in good agreement with the energies of scalar mode giant resonances [4] and so are the other characteristics of importance.

As an analogue to our derivations referred here as a zero-sound vibrations coupled to dynamic surface one can consider the traditional approximation of chaotic phases. So, in the right portion of Fig. 3 the dynamical density $\rho_d(r)$ calculated by means of (38, 40) is compared with the same quantity for lead for the first $l=2$ and $l=0$ resonance determined by RPA theory in which Hartree-Fock basis states and interaction S I was used [20]. Here, radius $R=6.8$ fm and $\beta=64$ MeV·fm^5. Roots of the characteristic equation (40) are: $kR=2.28$, 5.95 for $l=0$ and 1.38, 5.28 for $l=2$ for curves marked as a and b in the figure. Agreement with the detailed theory is, again, rather close.

The shapes of radial distribution functions shown in Fig. 3 support classification of nuclear vibrations as surface mode (a) volume mode (b, c, ...) resonances. For the volume type of vibrations the characteristic values of kR are close to roots of spherical Bessel functions. For the quadrupole type hydrodynamical surface vibrations $kR\ll 1$ whereas for zero-sound-plus-surface mode $kR=1.2$–1.4. Other important features of resonances are represented by the so-called model-less sum rules and response functions. These quantities are dealt with in a separate publication [21].

4. Conclusions

It has been shown that close descriptions of static and dynamical densities in heavy nuclei can be obtained in a simple approximation dealing with volume quantities coupled to diffused surface by means of boundary conditions set an a certains effective sharp surface.

Authors express their gratitude to I. Yu. Tzechmistrenko who performed some hydrodynamical calculations. All other results reported in this paper were obtained by means of TI-59 pocket calculator.

References

1. Wilets, L.: Phys. Rev. **101**, 1805 (1956); Rev. Mod. Phys. **30**, 542 (1958)
2. Strutinsky, V.M., Magner, A.G., Brack, M.: Z. Phys. A – Atoms and Nuclei **319**, 205 (1984)
3. Bethe, H.: Annu. Rev. Nucl. Sci., **21**, 93 (1971)
4. Strutinsky, V.M., Magner, A.G., Denisov, V.Yu.: Z. Phys. A – Atoms and Nuclei **315**, 301 (1984)
5. Strutinsky, V.M., Tyapin, A.S.: Exp. Theor. Phys. (USSR) **18**, 664 (1964)

6. Strutinsky, V.M.: a) Nucl. Phys. A **95**, 420 (1967); b) Nucl. Phys. A **122**, 1 (1968)
7. Ring, P., Schuck, P.: The nuclear many-body problem. Berlin, Heidelberg, New York: Springer-Verlag 1980
8. Brack, M.: Habilitationsschrift. Institut Laue Langevin, Grenoble 1977
9. Skyrme, T.H.R.: Philos. Mag. **1**, 8th ser., 1043 (1956)
10. Blaizot, J.P.: Phys. Rep. **64**, 172 (1980)
11. Barrett, R.C., Jackson, D.F.: Nuclear sizes and structure. Oxford: Clarendon Press 1977
12. Vautherin, D., Brink, D.: Phys. Rev. C **5**, 626 (1972)
13. Beiner, M., Flocard, H., Nguyen Van Giai, Quentin, P.: Nucl. Phys. A **238**, 29 (1975)
14. Eckart, G., Holzwarth, G., Da Providencia, J.P.: Nucl. Phys. A **364**, 1 (1984)
15. Kolomietz, V.M., Ofengenden, S.R., Tsekhmistrenko, I.Yu.: Yad. Fiz. **39**, 1356 (1984)
16. Strutinsky, V.M., Magner, A.G.: Sov. J. Part. Nucl. **7**, 138 (1977)
17. Jennings, B.K., Bhaduri, R.K., Brack, M.: Nucl. Phys. A **253**, 29 (1975)
18. Bohr, A., Mottelson, B.: Nuclear structure. Vol. 2. New York: Benjamin Inc. 1975
19. Kolomietz, V.M., Tsekhmistrenko, I.Yu.: Izv. Akad. Nauk USSR, Ser. Fiz. **49**, 985 (1985)
20. Bertsch, G.F., Tsai, S.F.: Phys. Rep. **18**, 125 (1975)
21. Magner, A.G., Denisov, V.Yu., Strutinsky, V.M.: (to be published)

V. Strutinsky
A. Magner
V. Denisov
Institute for Nuclear Research
Prospekt Nauki 119
SU-252028 Kiev-28
USSR